AGU PUBLICATIONS

JGR

Journal of Geophysical Research: Oceans

RESEARCH ARTICLE

10.1002/2013JC009476

Impacts of canonical and Modoki El Niño on tropical Atlantic SST

Dillon J. Amaya[1] and Gregory R. Foltz[2]

[1]Department of Atmospheric Science, Texas A&M University, College Station, Texas, USA, [2]NOAA/Atlantic Oceanographic and Meteorological Laboratory, Miami, Florida, USA

Key Points:
- Canonical El Niño causes warming in tropical N. Atl. with peak in MAM
- Response to Modoki is weaker overall and includes cooling in the NE tropical Atlantic
- Difference due to stronger PNA pattern and stronger eq Kelvin wave for canonical

Correspondence to:
G. R. Foltz
gregory.foltz@noaa.gov

Citation:
Amaya, D. J., and G. R. Foltz (2014), Impacts of canonical and Modoki El Niño on tropical Atlantic SST, *J. Geophys. Res. Oceans*, *119*, 777–789, doi:10.1002/2013JC009476.

Received 30 SEP 2013
Accepted 2 JAN 2014
Accepted article online 7 JAN 2014
Published online 7 FEB 2014

Abstract The impacts of canonical and Modoki El Niño on tropical Atlantic sea surface temperature (SST) are quantified using composite analysis. Results show that El Niño Modoki fails to produce significant warming in the tropical Atlantic, in contrast to the well known warming following canonical El Niño events. El Niño Modoki instead induces significant cooling in the northeastern tropical Atlantic and near-neutral conditions elsewhere in the tropical Atlantic. It is shown that the difference in SST response stems primarily from a much stronger Pacific/North American (PNA) teleconnection pattern and stronger atmospheric Kelvin wave response during canonical events compared to Modoki. The stronger PNA pattern and Kelvin waves during canonical events generate anomalously weak surface winds in the tropical North Atlantic, driving anomalously weak evaporative cooling and warmer SSTs. Past research has shown significant decadal variability in the frequency of noncanonical El Niños relative to canonical events. If such variability continues, it is likely that the impact of El Niño on tropical Atlantic SST will also fluctuate from one decade to the next.

1. Introduction

El Niño is a pattern of anomalously warm sea surface temperature (SST) in the equatorial Pacific that impacts global weather and climate through atmospheric teleconnections [*Horel and Wallace*, 1981; *Kiladis and Diaz*, 1989; *Yulaeva and Wallace*, 1994]. Strong El Niño events have been linked to a strengthening of the Pacific/North American (PNA) pattern, namely a deepening of the Aleutian Low, above-average heights over the intermountain region of North America, and below-average heights over the southeastern United States [*Wallace and Gutzler*, 1981]. Anomalous warming in the tropical Pacific Ocean associated with an El Niño heats the troposphere sufficiently to force a pronounced atmospheric Kelvin wave response [e.g., *Horel and Wallace*, 1981; *Chiang and Sobel*, 2002]. The Kelvin wave propagates eastward over South America to the tropical Atlantic and may force a stationary baroclinic Rossby wave, depicted in *Gill*'s [1980] model of tropical atmospheric circulations.

Anomalously low heights over the southeastern United States, forced by the PNA pattern, act to weaken the semipermanent subtropical high over the North Atlantic [e.g., *Horel and Wallace*, 1981]. Atmospheric Kelvin waves warm the troposphere over the tropical Atlantic anomalously, increasing static stability [e.g., *Chiang and Sobel*, 2002; *Lee et al*., 2011]. The associated stationary Rossby waves amplify the PNA-induced weakening of the subtropical high over the southeastern United States. The combination of midlatitude and equatorial teleconnections tends to weaken the northeasterly trade winds in the tropical North Atlantic, reducing evaporative cooling of the ocean's surface and increasing SST [*Carton et al*., 1996; *Enfield and Mayer*, 1997]. The anomalously warm SST in the tropical North Atlantic tends to peak in boreal spring, approximately one season after the typical peak of an El Niño event in boreal winter [*Enfield and Mayer*, 1997].

In recent years, a growing body of research has emphasized the existence of noncanonical or "nontraditional" flavors of ENSO. These noncanonical ENSO events are referred to as dateline, central Pacific, warm-pool, or Modoki El Niño in the literature [e.g., *Yeh et al*., 2009; *Ashok et al*., 2007; *Kao and Yu*, 2009; *Kug et al*., 2009; *Chiang and Vimont*, 2004; *Trenberth and Stepaniak*, 2001]. Modoki ENSOs are characterized by the warmest (coolest) SST anomalies in the central equatorial Pacific during El Niño (La Niña) events. During a Modoki El Niño, warm SST anomalies are often accompanied by anomalously cold SSTs to the east and west, forming a distinctive horseshoe pattern [*Ashok et al*., 2007].

Larson et al. [2012] showed that SST anomalies in the tropical Pacific associated with noncanonical events do not significantly affect hurricane activity in the tropical Atlantic during boreal summer and fall. They

© 2014. American Geophysical Union. All Rights Reserved.

concluded that noncanonical events are not strong enough to generate the increases in wind shear and atmospheric static stability in the tropical Atlantic necessary to suppress hurricane activity. In contrast, canonical events have been observed to decrease static stability and wind shear and hence decrease hurricane activity [e.g., *Goldenberg and Shapiro*, 1996; *Tang and Neelin*, 2004; *Klotzbach*, 2011a]. *Rodrigues et al*. [2011] showed that "strong and long" El Niños, with strongest heating in the eastern Pacific, lead to a reduction in rainfall in Northeast Brazil. In contrast, "weak and short" El Niños, with warming concentrated in the central Pacific, tend to enhance Northeast Brazil rainfall. The different rainfall responses were attributed to different SST responses in the eastern equatorial and tropical South Atlantic since SST anomalies in the tropical North Atlantic tended to be positive for eastern and central Pacific El Niños. Their results were based mainly on numerical model experiments and limited observational data (1957–2002), and the emphasis was on El Niño events that generated significant rainfall anomalies in Northeast Brazil.

In this study we focus on the impacts of canonical and Modoki El Niños on tropical Atlantic SST during boreal winter through summer. Boreal winter and spring are when the interhemispheric gradient of SST associated with the Atlantic Meridional Mode is most pronounced and its impacts on continental rainfall are strongest [*Hastenrath and Heller*, 1977; *Chiang et al*., 2002], and boreal summer corresponds to the first half of the Atlantic hurricane season. It is therefore important to understand the impacts of canonical and Modoki El Niño on tropical Atlantic SST during these seasons.

In recent decades, noncanonical events have grown in frequency compared to canonical events [*Yeh et al*., 2009; *Ashok et al*., 2007; *Kao and Yu*, 2009; *Kug et al*., 2009; *Lee and McPhaden*, 2010]. In order to understand the connections between the equatorial Pacific and the tropical Atlantic in a changing climate, it is therefore important to quantify the impacts of canonical and Modoki El Niño on tropical Atlantic SST. This study uses observed satellite and reanalyzed data sets to investigate differences in the response of tropical Atlantic SST to canonical and Modoki El Niño.

2. Data and Methods

We use monthly mean SST from NOAA's Extended Reconstructed Sea Surface Temperature Version 3b (ERRST.v3b), which is available from 1854-present [*Smith et al*., 2008]. The ERSST.v3b data set extending back more than a century has been used successfully in past El Niño studies [e.g., *Yeh et al*., 2009; *Messié and Chavez*, 2011]. Monthly mean surface wind velocity, 500 mb heights, and surface solar radiation were obtained from NOAA's Twentieth Century Reanalysis Version 2 (20CR.v2), available from 1871 to 2011 [*Compo et al*., 2011]. Monthly mean tropospheric temperatures were also taken from the 20CR.v2 at 17 pressure levels from 1000 to 200 mb. Mean tropospheric temperatures were calculated as the average over all pressure levels. Both data sets are available on a 2°x2° grid. We restrict our analysis to the 1880–2010 period, when ERSST is most reliable. Data prior to 1880 also contain very little year-to-year variability and consequently would not add value to our analysis [*Smith and Reynolds*, 2003].

We perform a composite analysis of SST anomalies starting from January 1880 and ending in December 2010. The monthly mean climatology was first calculated for the 1880–2010 period and removed from the SST time series at each grid point to obtain SST anomalies. Linear trends were then removed at each grid point for the whole time series. El Niño events tend to be phase locked to the seasonal cycle such that they peak in boreal winter [e.g., *Tziperman et al*., 1998]. Canonical El Niño events were therefore defined when the DJF SST anomaly in the Niño-3 region (90°W–150°W, 5°S–5°N) was greater than 0.5 times the standard deviation of the Niño-3 Index (the standard deviation is ~1°C). This low threshold was chosen in order to increase the sample size and hence the statistical robustness of our results. To test our results' sensitivity to the season used to define events (e.g., NDJ as opposed to DJF), the analysis was repeated for events peaking in NDJ and NDJF. Results were consistent for each defining season; however, DJF yielded the most statistically robust composites. Table 1 shows the canonical El Niño events based on our methodology.

Modoki events were defined when the El Niño Modoki Index (EMI) [*Ashok et al*., 2007] (see Figure 1b) was greater than 0.5 times its standard deviation (the standard deviation is ~0.4°C):

$$\mathrm{EMI} = |\mathrm{SSTA}|_A - 0.5 * |\mathrm{SSTA}|_B - 0.5 * |\mathrm{SSTA}|_C, \quad (1)$$

We choose a threshold of 0.5 standard deviations for consistency with the definition used for canonical events. Here |SSTA| is the average SST anomaly in regions A (10°S–10°N, 165°E–140°W), B (15°S–5°N,

© 2014. American Geophysical Union. All Rights Reserved.

Table 1. Onset Years for Significant DJF Events (i.e., the Year 1880 Corresponds to the Event That Peaked During December 1880–February 1881)[a]

	Niño-3	*EMI*	*Niño-4*
	1880, 1884, 1887, 1895, 1888, 1895, 1899, 1905, 1911, 1918, 1919, 1930, 1939, 1951, 1969, 1976, 1982, 1987, 1997, 2003, 2006	1883, **1923, 1929,** 1953, **1958**, **1977**, 1979, **1990**, 1992, 1993, 2001, 2004	1883, 1907, **1923**, **1929**, **1958, 1977,** 1979**, 1990,** 1992, 2001, 2004
Total	*21*	*12*	*11*
	TNI	***PMM***	***CPW***
	1883, 1900, 1907, **1923**, 1927, **1929**, 1935, 1946, 1948, 1953, 1**958**, **1977**, 1979, 1989, **1990**, 1996, 2001, 2004	1885, 1890, 1900, 1907, **1923,** 1927, **1929**, 1935, **1958, 1977,** 1979**, 1990,** 1992, 1993, 1996	1883, 1907, **1923**, **1929**, **1958**, 1968, **1977, 1990**, 1992, 1994, 2001, 2004
Total	*18*	*15*	*12*

[a]See text for definition of each index. Bold indicates common year among all non-canonical indices. Total shows number of years going into the composite for each index. For simplification, we show only the unique Niño-3 events relative to EMI events.

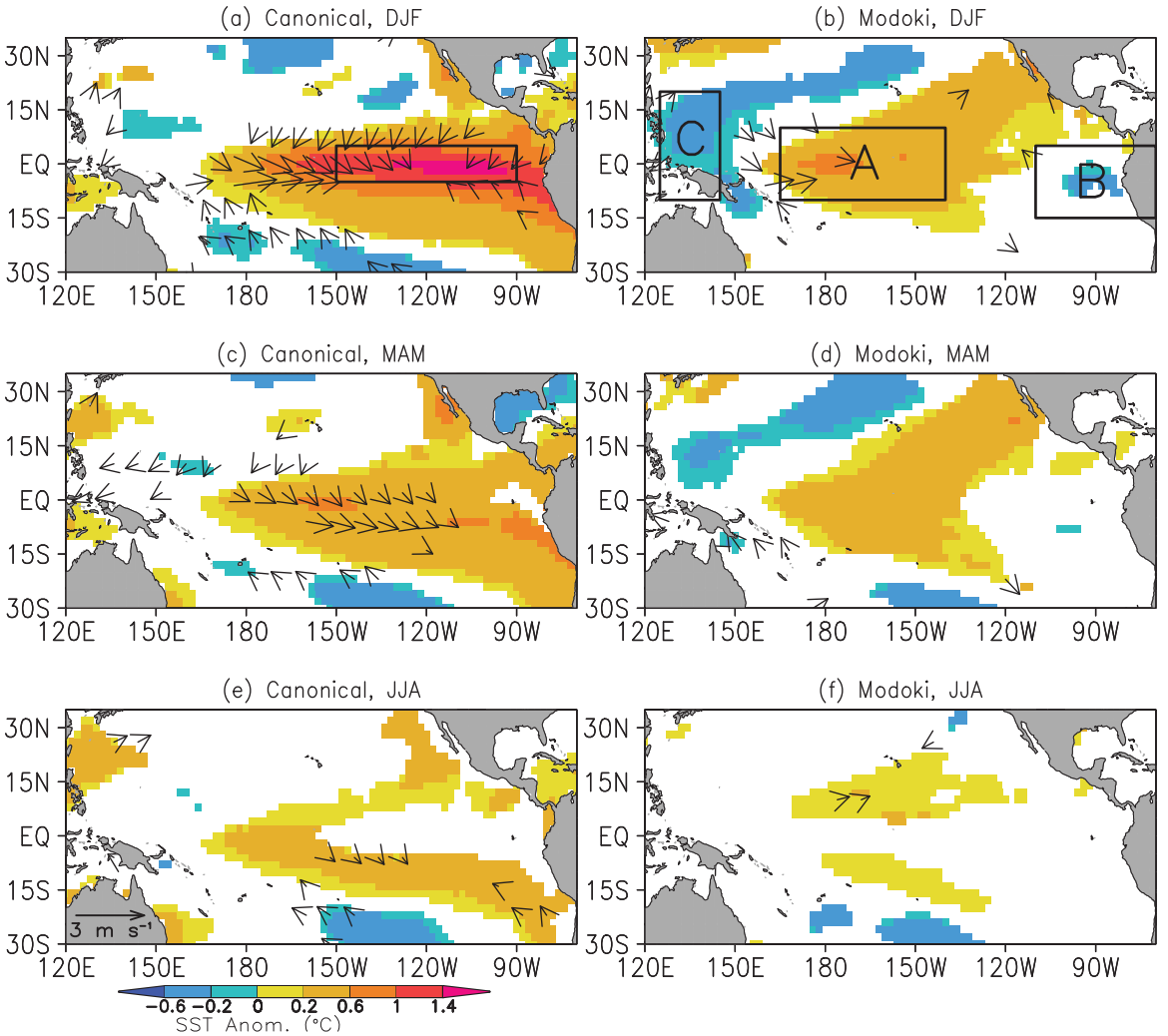

Figure 1. Composites of SST and surface wind anomalies for 21 canonical and 12 Modoki El Niño events running from the event peak in DJF to the following JJA. SST and wind vectors shown are significant at the 10% level based on a Student's one sample *t* test. Boxes in Figures 1a (1b) outline Niño-3 (EMI) regions.

© 2014. American Geophysical Union. All Rights Reserved.

110°W–70°W), and C (10°S–20°N, 125°E–145°E) (see Figure 1b). To avoid confusing Modokis with strong canonical El Niño or La Niña events, we use the criterion that DJF $|SSTA|_A$ has to be greater than 0.5 times the standard deviation of SSTA in region A (the standard deviation is ~0.6°C) [*Tedeschi et al*., 2013]. This emphasizes the SST anomalies in the central Pacific relative to the flanking opposite-signed signals. Table 1 shows the Modoki events according to our definition.

For each index, a composite of SST anomalies in DJF was created by averaging all events during DJF that were greater than the index's respective threshold. To investigate the conditions following the peak of a composite El Niño in DJF (either canonical or Modoki), lag composites were calculated for 3 month seasons ranging from MAM to SON the following year. Surface winds drive SST variability in the tropical Atlantic, with winds leading by about 2 months [*Carton et al*., 1996; *Czaja et al*., 2002]. To investigate the mechanisms driving the SST variability in the tropical Atlantic, we therefore shift the lead/lag composites for surface winds, 500 mb height, mean tropospheric temperature, and surface solar radiation such that each 3 month average leads the corresponding SST season by 2 months (i.e., JFM for surface winds, height, temperature, and shortwave corresponds to MAM for SST, etc.). We use only the years when there was a significant canonical/Modoki event in DJF.

Other indices used to define warm events in the central equatorial Pacific include the Niño-4 index (SST anomaly averaged between 5°S and 5°N and 160°E and 150°W), Trans-Niño Index (TNI) [*Trenberth and Stepaniak*, 2001], Pacific Meridional Mode (PMM) [*Chiang and Vimont*, 2004; *Larson et. al*., 2012] and Central Pacific Warming (CPW) [*Yeh et al*., 2009]. In this study we focus on the differences between Modoki and canonical El Niño because we believe that the Modoki index best captures the contrast between central and eastern Pacific warm events. However, since there is not a consensus on which index best captures noncanonical El Niño variability, we repeat our analysis for each of the noncanonical indices mentioned above.

The TNI index is calculated as:

$$\mathrm{TNI} = [[\mathrm{Ni\tilde{n}o}-4]-[\mathrm{Ni\tilde{n}o}-1+2]], \tag{2}$$

where the Niño-1+2 region is (10°S–0°N, 90°W–80°W) and [] represents normalization. In (2) the difference has been reversed relative to *Trenberth and Stepaniak* [2001] so that a positive value corresponds to a warm event in the central/western equatorial Pacific [e.g., *Larson et al*., 2012]. The PMM index is calculated as:

$$\mathrm{PMM} = [[\mathrm{ENP}]-[\mathrm{Ni\tilde{n}o}-1+2]], \tag{3}$$

where ENP is the eastern North Pacific region (10°N–30°N, 140°E–110°W). A positive PMM event is therefore characterized by an anomalous northwestward SST gradient across the mean position of the Pacific intertropical convergence zone. The SST anomaly in the ENP region for a PMM event typically extends southwestward to the central equatorial Pacific (165°E–140°W), which is where the positive SST signals associated with El Niño Modokis tend to be largest.

The CPW events are calculated by first determining when the area averaged SST anomaly over the Niño-4 region is greater than 0.5°C or when the area averaged SST anomaly over the Niño-3 region is greater than 0.5°C. If the Niño-4 (Niño-3) region is above 0.5°C, but the Niño-3 (Niño-4) is not for a given DJF, that year is still defined as an event. For each of these events, if Niño-4 is greater than Niño-3 and Niño-4 is positive, then a central Pacific warming event exists [e.g., *Yeh et al*., 2009]. *Yeh et al*. [2009] used a threshold of 0.5°C for CPW. To be more consistent with the EMI defined previously in this section and to obtain enough events for a robust composite, we reduced the threshold to 0.3°C. The years in which the various noncanonical El Niños occurred are shown in Table 1.

Our analysis focuses on the differences between canonical and Modoki El Niños based on the Niño-3 Index and the EMI. Because there is some overlap in the regions used to define each index (Figure 1), it is possible that a canonical event and a Modoki event may be defined in a given year. In order to isolate the signal associated with each index, common years between canonical and Modoki events are omitted from the composites. Note that this qualification excludes the 2002–2003 El Niño event from our analysis since it is defined as a canonical and a Modoki event.

© 2014. American Geophysical Union. All Rights Reserved.

Table 2. Mean, Area-Averaged, Canonical Minus Noncanonical Values[a]

	EMI Difference (12)	Niño4 Difference (11)	TNI Diff. (18)	PMM Difference (15)	CPW Difference (12)
			SST (°C) for Region TA2		
DJF	0.17	0.18	0.1	0.18 (0.20)	0.13
MAM	**0.33 (0.05)**	**0.34 (0.05)**	**0.24 (0.10)**	**0.26 (0.10)**	**0.27 (0.10)**
JJA	**0.26 (0.05)**	**0.25 (0.05)**	**0.18 (0.10)**	**0.20 (0.05)**	**0.23 (0.05)**
			Winds (m/s) for Region TA2		
OND	0.03	0	−0.07	**−0.19 (.10)**	0
JFM	**−0.29 (0.10)**	−0.25 (0.20)	**−0.26 (0.10)**	**−0.28 (0.10)**	−0.18
AMJ	0.08	0.06	0.01	−0.04	−0.02
			Tropospheric Temperature (K) for Region TA3		
OND	0.13	0.17 (0.20)	0.07	0.12 (0.20)	0.09
JFM	**0.34 (0.01)**	**0.35 (0.01)**	**0.31 (0.01)**	**0.32 (0.01)**	**0.26 (0.05)**
AMJ	*0.16 (0.20)*	0.17 (0.20)	**0.18 (0.10)**	**0.20 (0.05)**	0.11
			500 mb Height (m) for Region TA1-Region TA2		
OND	−5.22 (0.20)	−4.73	−3.27	−3.27	−2.87
JFM	**−14.38 (0.05)**	**−13.07 (0.10)**	**−16.62 (0.01)**	**−16.76 (0.05)**	−12.05 (0.20)
AMJ	−0.76	−0.44	−2.01	−1.37	−0.5

[a]Columns represent each noncanonical index. *P* values of a Student's two-sample *t* test between each canonical and noncanonical index are in parentheses if they are 20% or less. Only values of 1%, 5%, 10%, and 20% are shown. Bold represents area averages that are significant at the 10% level. The number of events going into each noncanonical composite is in parenthesis next to the respective column heading. For each column, common events are excluded from the canonical and the noncanonical composites used to calculate differences. Figure 5d shows the TA regions.

Statistical significance between a canonical and Modoki composite is assessed using a Student's two-sample *t* test. Results are similar for other time periods (e.g., 1900–2010, 1920–2010) that give at least eight unique DJF events for the given ENSO index. Results are also similar for other thresholds (multiples of the standard deviation of 0.3–0.7), and for other noncanonical indices, as discussed in the following section and shown in Tables 1 and 2.

3. Results

Composites of SST anomalies in the tropical Pacific from the boreal winter (DJF) peak of a canonical or Modoki event until the boreal summer (JJA) after the peak of the event generally agree with previous results (Figure 1). The canonical and Modoki El Niños peak in boreal winter, with the warmest SST anomalies concentrated in the East Pacific for canonical and near the dateline for Modoki. Surface winds also converge anomalously during boreal winter, consistent with anomalous eastward shifts of deep convection and the rising branch of the Walker Circulation [*Bjerknes*, 1969]. SST and surface wind anomalies are much weaker for Modoki compared to canonical, consistent with previous results [*Ashok et al*., 2007]. During the boreal spring and summer seasons (MAM and JJA) following the winter peak, canonical and Modoki events begin to decay, with most of the SST anomalies trending toward zero or slightly negative going into boreal summer. As expected, the intensity of surface wind convergence for canonical and Modoki diminishes from the spring to summer in response to the cooling SST.

Composites of SST and surface winds in the tropical Atlantic for canonical El Niño events are generally consistent with results from previous studies (Figure 2). For canonical events, anomalous warming builds up in boreal winter and peaks across the tropical North Atlantic basin during March-May (Figures 2a and 2b). Anomalous southwesterly surface winds during the winter weaken the northeasterly trade winds, decreasing evaporative cooling and leading to the boreal spring peak in anomalous SST. A lack of anomalous surface wind forcing allows warm SST anomalies to weaken in the summer and diminish further by the following fall (SON) (Figures 2c and 2d).

In contrast, Modoki El Niño events do not generate significant warming in the tropical North Atlantic (Figure 3). Instead, there are near-neutral SST anomalies in the northwestern, equatorial, and southeastern tropical Atlantic and anomalous cooling in the eastern tropical North Atlantic. During October-December anomalously strong northeasterly surface winds are present in a band running from 17°N to 35°N and 15°W to 45°W (Figure 3a). The enhanced wind speed drives an anomalous increase in evaporation and anomalously cold SSTs in boreal winter (DJF), 2 months later. Below average SSTs intensify during boreal spring around 25°N–35°N, 15°W–30°W (Figure 3b). The negative SST anomalies propagate southwestward and peak during the spring and summer, covering the region 15°N–35°N, 15°W–40°W (Figure 3c). The

© 2014. American Geophysical Union. All Rights Reserved.

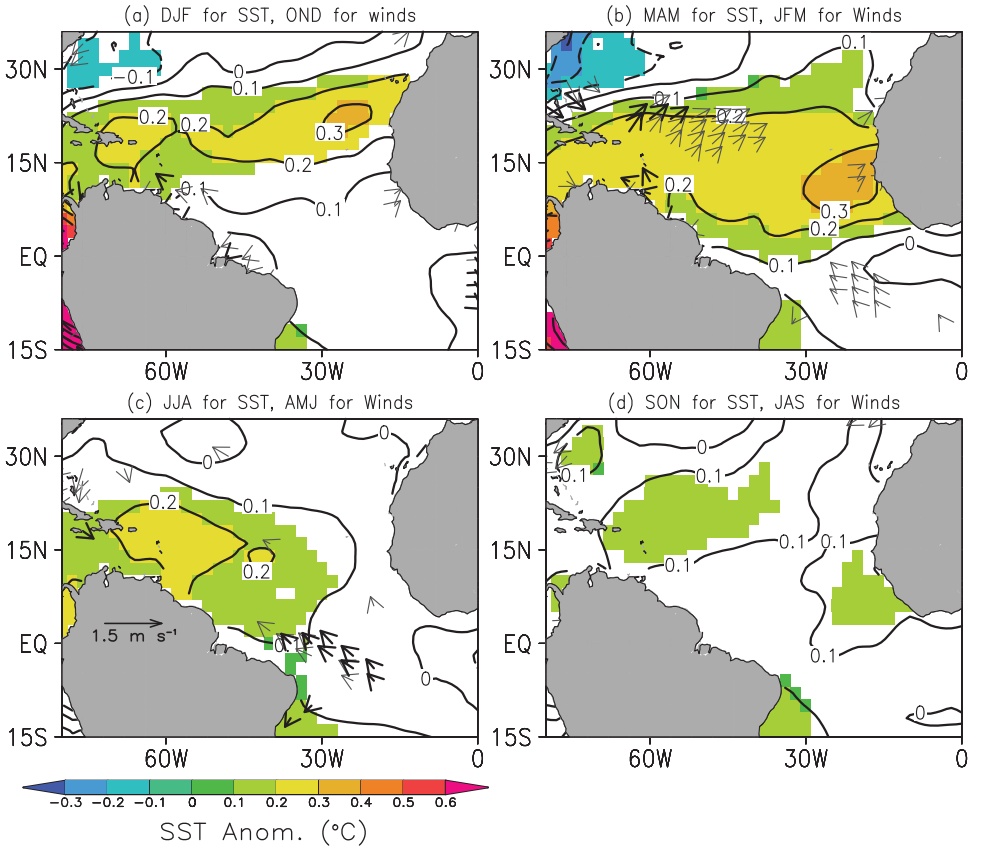

Figure 2. Canonical El Niño lag composites of SST anomalies (contours and shading) and lead/lag composites of surface winds (vectors) for (a) DJF, (b) the MAM following the peak in DJF, (c) the following JJA, and (d) the following SON. The SSTA values shown in color are significant at the 10% level based on a Student's one sample *t* test of 21 events. Black wind vectors lead SST by 2 months (e.g., JFM winds for MAM SST) and are significant at the 10% level. Gray vectors are significant at the 20% level.

surface wind forcing of the cool SST anomalies appears to occur primarily during October-March and drops off quickly by April-June. As a result, significantly cold SST anomalies in the tropical North Atlantic dissipate by the following fall (SON) (Figure 3d).

For the canonical and Modoki composites, the SST anomalies in the tropical North Atlantic are more widespread and spatially coherent than the wind anomalies, suggesting that other processes besides wind-induced evaporative cooling may contribute significantly to the anomalous changes in SST. Changes in the surface air-sea humidity and temperature gradients (i.e., the "tropospheric temperature" or "backpressure" mechanisms) [*Brown and Bretherton*, 1997; *Chiang and Sobel*, 2002; *Chiang and Lintner*, 2005] and changes in surface solar radiation [*Tanimoto and Xie*, 2002; *Foltz and McPhaden*, 2006] have been shown to induce anomalous warming in the tropical North Atlantic following El Niño events and may explain the stronger SST responses relative to the surface wind responses.

For the canonical composite there is a zonal band of positive surface solar radiation anomalies centered near 15°N during October-March, which would tend to enhance the positive SST anomalies in the same region during boreal winter and spring (Figure 4). There are also negative anomalies of solar radiation in the eastern tropical North Atlantic during April-June that are consistent with the pronounced decrease in the strength of warm SST anomalies in that region between March-May and June-August (Figures 2b, 2c, and 4c). For the Modoki composite, the three to six month lag between the largest surface wind anomalies and cold SST anomalies, and the southwestward movement of the SST anomalies, may be due in part to an area of negative surface solar radiation anomalies between 0° and 20°N during January-March (not shown). The increase in solar radiation for canonical events and reduction for Modoki are consistent with positive SST-low cloud-shortwave radiation feedback (i.e., an increase in SST leads to a decrease in cloudiness and

© 2014. American Geophysical Union. All Rights Reserved.

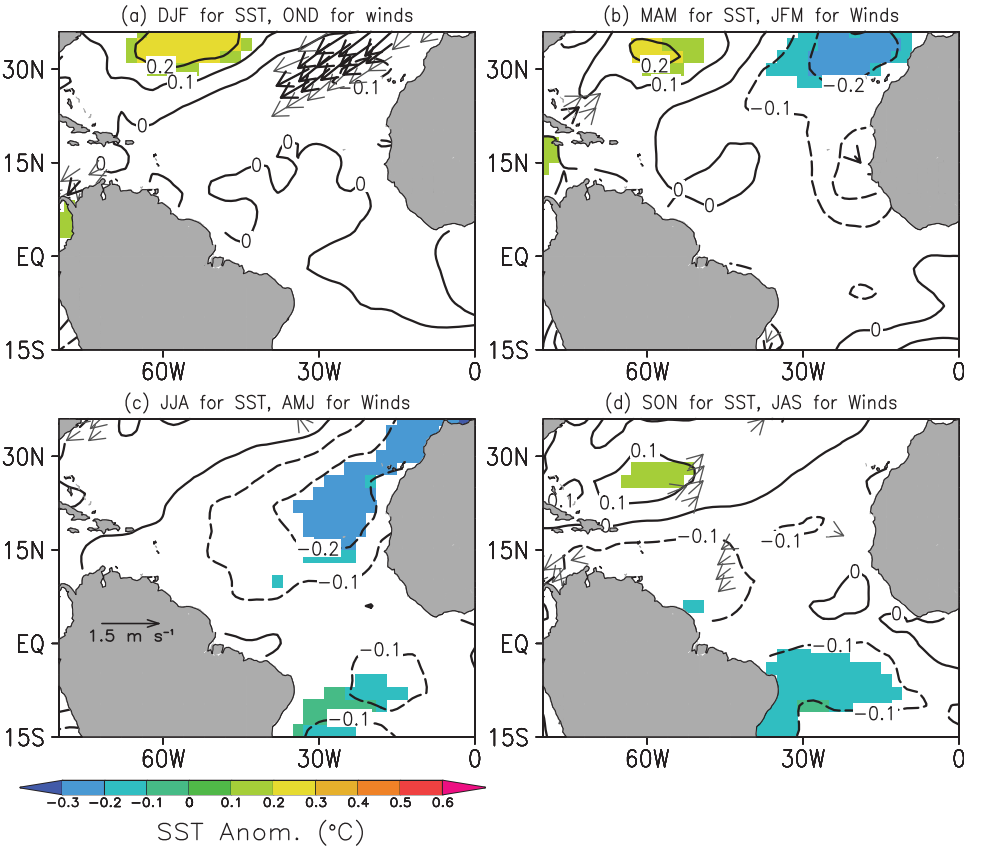

Figure 3. As in Figure 2, except composites of 12 Modoki events.

an increase in solar radiation) [*Tanimoto and Xie*, 2002]. However, these results should be viewed with caution because of the lower quality of the solar radiation data in comparison to SST and surface winds.

The differences in SST and surface winds in the tropical North Atlantic for canonical minus Modoki are shown in Figure 5. During October-December (two months prior to the boreal winter season), canonical events drive anomalously southwesterly winds between 20°N and 35°N, relative to Modoki (Figures 2 and 3), weakening the mean northeasterly trade winds, reducing evaporative cooling, and warming SSTs (Figure 5a). In boreal winter the entire tropical Atlantic from 15°S to 30°N is anomalously warm, with the most significant anomalies extending across the tropical North Atlantic basin between about 15°N and 30°N and 25°W and 60°W. There is evidence that the winds are responding to the anomalous meridional SST gradient during October-December. Indeed, a consistent anomalous interhemispheric SST gradient in the tropical Atlantic in September-February for canonical relative to Modoki forces anomalously cross-equatorial surface winds over a broad region from about 0°N to 10°N and 25°W to 70°W (Figure 5a).

Southwesterly surface wind anomalies spread and intensify during January-March leading up to the boreal spring season, driving weaker northeasterly trade winds and less evaporative cooling across the basin (Figure 5b). Ultimately, this drives significantly more anomalous warming of the tropical North Atlantic (about 0°–25°N, 20°W–60°W) for canonical events relative to Modoki events during boreal spring, and the peak warming is shifted southward to about 5°N–15°N, 20°W–30°W during this season. The positive SST differences in the tropical North Atlantic result from the combination of anomalous warming for canonical and anomalous cooling for Modoki (Figures 2 and 3). There are also positive anomalies of surface solar radiation during this season that may contribute to the observed warming for canonical relative to Modoki, though the anomalies are confined mainly to the central tropical North Atlantic (30°W–50°W, 10°N–20°N; not shown).

The following summer (JJA) shows a decrease in the canonical minus Modoki SST warming (Figure 5c). The peak of the anomalous warming has shifted southwestward to about 10°N–20°N, 25°W–65°W in response

© 2014. American Geophysical Union. All Rights Reserved.

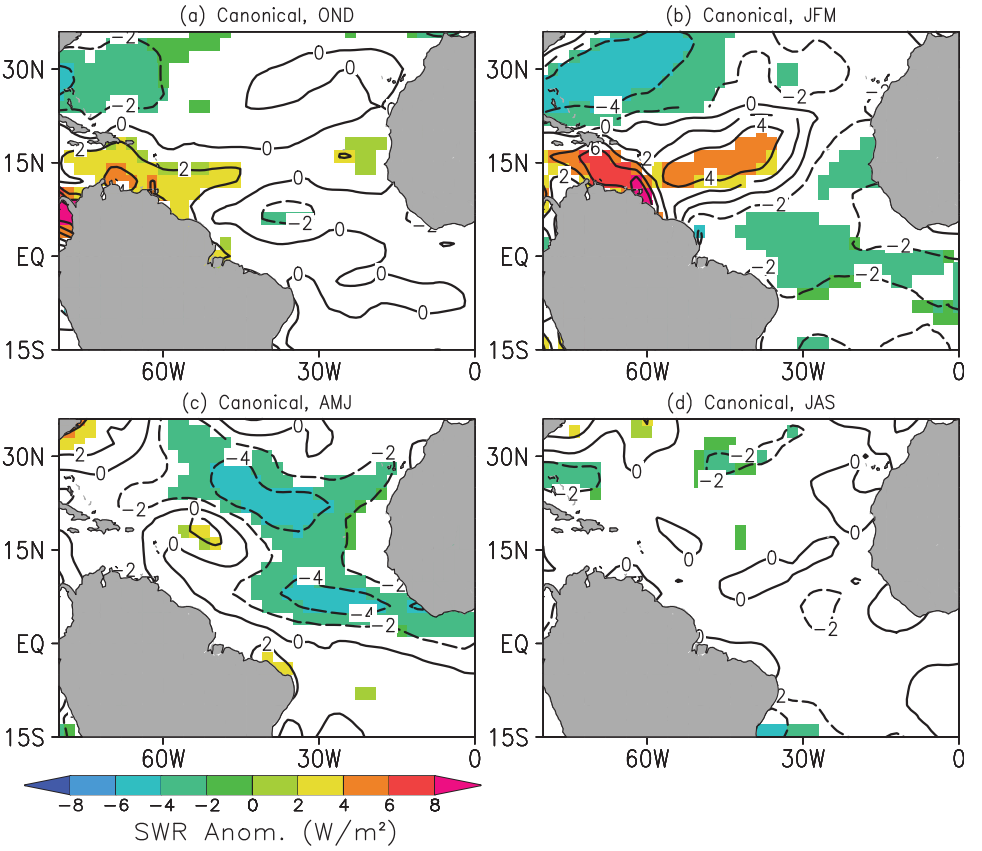

Figure 4. Canonical El Niño lead/lag composites of surface solar radiation anomalies (contours and shading) for (a) OND, (b) the following JFM, (c) the following AMJ, and (d) the following JAS. The SWRA values shown in color are significant at the 10% level based on a Student's one sample *t* test of 21 events.

to a westward shift in anomalous warming for canonical events and a southward shift in anomalous cooling in response to Modoki (Figures 2 and 3). The weakening and southwestward shift of the SST difference signal in boreal summer is also consistent with very weak anomalies of surface winds two months prior to the summer season (April-June) for canonical and Modoki and the tendency for SST anomalies in the tropical North Atlantic to propagate southwestward due to positive wind-evaporation-SST feedback [e.g., *Vimont*, 2010]. There are also indications of anomalous cross-equatorial surface winds in the west for canonical relative to Modoki (Figure 5c), where the anomalous meridional SST gradient is strongest.

During the following boreal fall (SON) the most significant SST anomalies in the tropical Atlantic for canonical El Niño relative to Modoki continue to shift southwestward (~15°N–30°N, 45°W–75°W), possibly due to a positive wind-evaporation-SST feedback (Figure 5d) [*Smirnov and Vimont*, 2012]. The surface wind response is minimal in the July-September period leading up to boreal fall.

The main mechanisms through which El Niño influences the tropical Atlantic are the indirect, midlatitude PNA pattern and the more direct equatorial atmospheric Kelvin wave response. In order to explore the causes of the significant differences in wind and SST responses to canonical events relative to Modoki, Figure 6 shows the height of the 500 mb pressure surface and tropospheric temperature, illustrating the PNA and Kelvin wave mechanisms, respectively. We focus on the October-December and January-March seasons because we are interested in the forcing mechanisms for the strongest SST signals in the tropical North Atlantic during boreal winter (December-February) and spring (March-May), and we expect the forcing to lead the SST by about 2 months.

In October-December, the canonical composite of 500 mb height shows an anomalous deepening of the Aleutian Low, consistent with the development of a positive PNA pattern, and above-average heights extending from 30°S to 30°N in the tropical Atlantic (Figure 6a). In contrast, the Modoki composite does

© 2014. American Geophysical Union. All Rights Reserved.

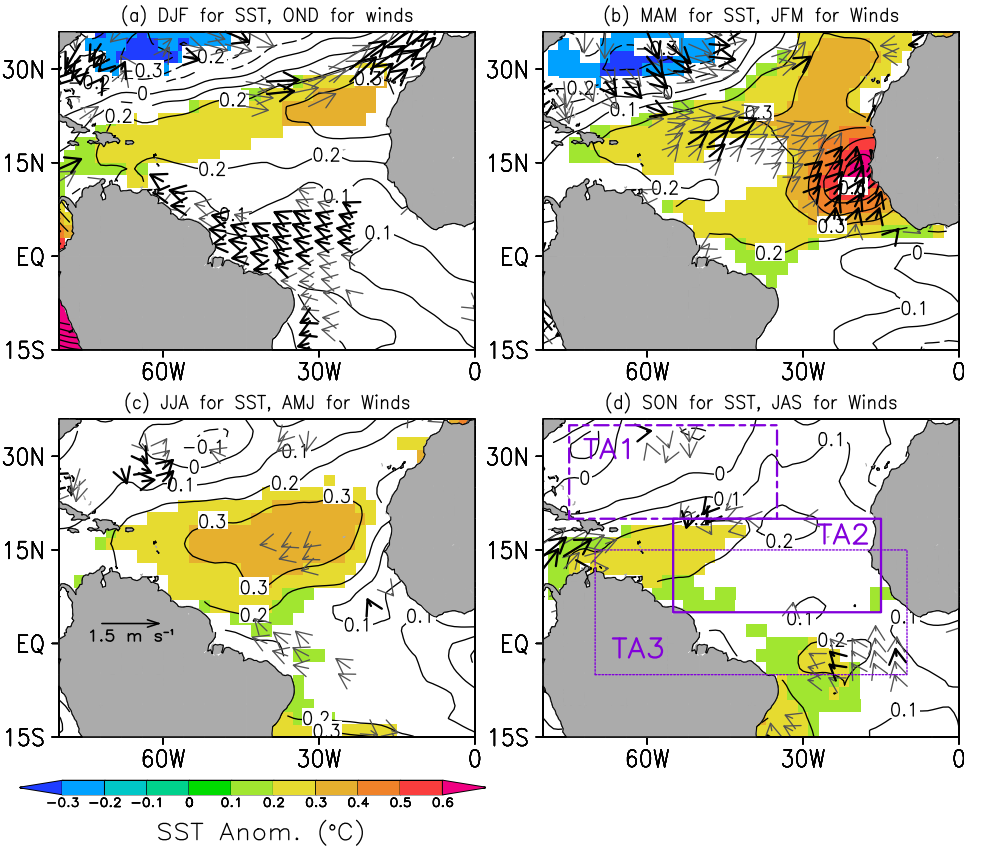

Figure 5. Modoki lag composites of SST anamolies (contours and shading) and surface winds (vectors), subtracted from the corresponding canonical composites for (a) DJF, (b) MAM following the El Niño peak in DJF, (c) the following JJA, and (d) the following SON. The SSTA values shown in color are significant at the 10% level based on a Student's two-sample *t* test of 21 canonical and 12 Modoki events. Black wind vectors lead SST by 2 months (e.g., JFM winds for MAM SST) and are significant at the 10% level. Gray vectors are significant at the 20% level. Tropical Atlantic (TA) boxes in Figure 5d represent regions of area averaging depicted in Table 2. TA1: 20°N–30°N, 35°W–75°W), TA2: (5°N–20°N, 15°W–55°W), and TA3: (5°S–15°N, 10°W–70°W).

not show a significant deepening of the Aleutian Low, and positive height anomalies extend only to ~10°N in the tropical North Atlantic (Figure 6b). In addition, heights are significantly above normal in the North Atlantic around 30°N–45°N, 25°W–75°W for Modoki, reminiscent of a positive phase of the North Atlantic Oscillation [*Barnston and Livezey*, 1987]. The strengthening of the subtropical high in this region is consistent with the strengthening of the northeasterly trade winds we see during October-December leading up to the cold SST anomalies (Figure 3a). As a result, the difference of canonical relative to Modoki shows an anomalously low height signal in the North Atlantic and an anomalously high height signal in the eastern tropical North Atlantic (Figure 6c). These two height anomalies are consistent with the anomalous southwesterly surface winds observed in October-December, which act to weaken the northeasterly trade winds, reduce evaporative cooling, and increase SST for canonical relative to Modoki, near 15°N–30°N, 20°W–60°W and during December-February (Figures 2, 3, and 5a).

The equatorial, atmospheric Kelvin wave propagates rapidly eastward after the initial forcing [e.g., *Chiang and Sobel*, 2002]. As a result, the October-December canonical El Niño composite shows an atmospheric Kelvin wave response in height and temperature that has already propagated eastward to the tropical Atlantic. Modoki forces a similar Kelvin wave response, though the signal is weaker, especially for tropospheric temperature, consistent with *Larson et al.* [2012]. However, the difference between canonical and Modoki does not show a significant signal in the equatorial Atlantic (Figure 6c).

In January-March, two months prior to the boral spring season (MAM), the composite of canonical events clearly shows the classic PNA pattern, with a deepened Aleutian Low, above-average heights over northern North America, and below-average heights over the southeastern United States. (Figure 6d). The below-average heights over the southeastern United States are consistent with the anomalous southwesterly

© 2014. American Geophysical Union. All Rights Reserved.

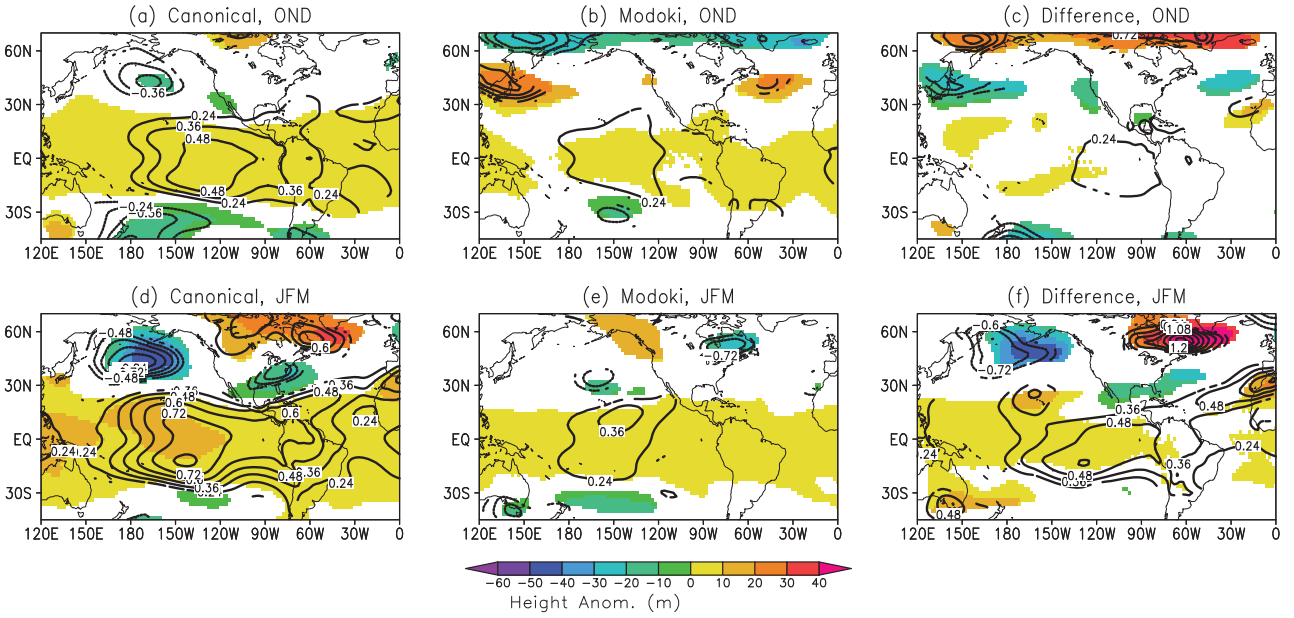

Figure 6. Lead/lag composites of 500 mb height (shaded) and tropospheric temperature (contoured) anomalies during (a)-(c) OND leading up to the El Niño peak in DJF and (d)-(f) the JFM during/after. Values are shown only where they are significant at the 10% level based on a Student's one sample t-test. The canonical-Modoki differences are shown in Figures 6c and 6f where they are significant at the 10% level based on a Student's two-sample *t* test of 21 canonical and 12 Modoki events.

surface winds we observe in the tropical North Atlantic during January-March for canonical events (Figure 2b). In contrast, the PNA pattern is absent in the Modoki composite. As a result, the canonical-Modoki difference closely mirrors the canonical composite, with lower heights in the subtropical North Atlantic and Gulf of Mexico (25°N–45°N, 45°W–120°W) and a northwest to southeast gradient of height across the tropical North Atlantic (Figure 6f).

The atmospheric Kelvin wave forced by the canonical composite strengthens in January-March. The height and tropospheric temperature signals can be seen throughout the entire tropical Atlantic from 30°S to 30°N (Figure 6d). A consequence of the Kelvin wave is the formation of a stationary baroclinic Rossby wave off the equator in the western tropical North Atlantic [*Gill*, 1980]. This feature will tend to amplify the intensity of the below-average heights over the southeastern U.S. Modoki El Niño does not force a comparable tropospheric temperature response over the tropical Pacific or the tropical Atlantic (Figure 6e). The canonical-Modoki differences reveal the greater intensity and more extensive eastward propagation of the tropospheric temperature anomalies for canonical relative to Modoki (Figure 6f). The most significant difference in tropospheric temperature is isolated in the tropical North Atlantic around 10°N–30°N, 10°W–70°W. A significantly warmer tropospheric temperature for canonical relative to Modoki in this region will tend to increase static stability and reduce convection, in turn reducing the strength of the northeasterly trade winds. Ultimately the PNA pattern, atmospheric Kelvin wave, and the baroclinic Rossby wave combine to force weaker northeasterly trade winds in January-March (resulting in less evaporative cooling) and the warm SSTs observed for canonical relative to Modoki between 0°N and 30°N and 25°W and 60°W during March-May (see Figure 5b).

To test the sensitivity of our results to the noncanonical index used, the previous analyses were repeated for a variety of noncanonical El Niño indices. Results for the canonical minus Modoki differences are shown in Table 2 for key regions in the tropical North Atlantic. For SST averaged in the region 5°N–20°N, 15°W–55°W results are generally consistent for all noncanonical indices. There is significant anomalous warming of SST in this region for canonical relative to noncanonical during boreal spring and summer. The intensity of the warming varies slightly, ranging from 0.25°C to 0.33°C. For each noncanonical index the warming results from the combination of anomalously warm SSTs for canonical and anomalous cooling for noncanonical (Figures 2 and 3). During January-March, 2 months before the boreal spring peak of warming for canonical relative to Modoki, there is a decrease in wind speed for canonical relative to the other noncanonical indices, with varying ranges of significance (Table 2). The reductions in wind speed in JFM for the

© 2014. American Geophysical Union. All Rights Reserved.

EMI, TNI, and PMM indices are all significant at the 10% level. Similar reductions in wind speed can be seen in the Niño-4 Index, though the statistical significance is not as high.

In order to capture the equatorial Kelvin wave signal in the tropical Atlantic for the noncanonical indices, tropospheric temperatures were averaged in the 5°S–15°N, 10°W–70°W region. There are significantly higher tropospheric temperatures for canonical events relative to noncanonical in this region during January-March leading up to boreal spring. Results are consistent across all noncanonical indices (Table 2). The values for October-December (leading boreal winter by 2 months) and April-June (leading boreal summer by 2 months) are also positive, with canonical minus noncanonical differences ranging from 0.13 to 0.20 K and significance varying from 5% to 20%. Finally, a northwest to southeast 500 mb height anomaly gradient was calculated by subtracting the area averaged values of canonical relative to noncanonical in the region 5°N–20°N, 15°W–55°W from the values in the region 20°N–30°N, 35°W–75°W (Figure 5d shows the regions). Results indicate a significant southeastward height gradient across the tropical North Atlantic during January-March (Table 2) that is consistent across all noncanonical indices except CPW.

To test whether the location of the peak warming for noncanonical indices in the tropical Pacific has a noticeable effect on tropical Atlantic SST, a third criterion was added to the EMI. In addition to meeting the criteria specified in Eq. (1), the ENP had to be below 0.6°C in order for a Modoki event to be included in the composite. This ensures that events going into the composite truly had peak warming in the central Pacific. We found that SST and wind anomalies in the tropical Atlantic were consistent when removing the influence of the ENP from the EMI composite, compared to the results with the standard EMI.

4. Summary and Discussion

The impacts of canonical and Modoki El Niño on tropical Atlantic SST were quantified using composite analysis. It was found that canonical El Niño generates significant warming in the tropical North Atlantic (5°N–25°N, 20°W–70°W) beginning in boreal winter, peaking in the spring, and persisting through the summer. These results are consistent with previous studies showing significant warming in the tropical Atlantic roughly one season following the peak of a canonical El Niño event in boreal winter [*Enfield and Mayer*, 1997]. In contrast, El Niño Modoki does not force comparable warming in the tropical Atlantic. Instead, there is significant, anomalous cooling in the northeastern tropical Atlantic during boreal spring through summer for Modoki.

The SST differences between canonical and Modoki were found to be significant during boreal winter through summer. The differences in boreal spring and summer stem from the combination of a stronger Pacific/North America teleconnection pattern and a stronger atmospheric Kelvin wave response for canonical events relative to Modoki, which decreases the strength of the tropical North Atlantic trade winds and increases SST. The stronger SST warming in the tropical North Atlantic during boreal winter can be traced to conditions during the preceding fall, when the combination of above-average heights in the North Atlantic for Modoki relative to canonical and below-average heights in the eastern subtropical North Atlantic force anomalously cyclonic surface winds in the eastern tropical North Atlantic. The result is a band of anomalously weak winds for canonical relative to Modoki, which tends to reduce evaporative cooling and increase SST.

The main conclusion of this study is that the impact of Modoki El Niño on tropical Atlantic SST is significantly different than the impact of canonical El Niño. The cause of the difference in atmospheric responses to different Pacific SST anomalies is unclear, since there seem to be two competing influences. On the one hand, the positioning of Modoki events closer to the climatological warm pool in the western equatorial Pacific would tend to result in a stronger atmospheric response for a given SST anomaly compared to the response for the same anomaly in the eastern equatorial Pacific associated with a canonical event. Alternately, Modoki events tend to be weaker relative to canonical events, so that the positioning of the warm anomaly in the equatorial Pacific may be secondary to the strength of the anomaly when it comes to forcing an atmospheric response capable of teleconnecting to the tropical Atlantic. Based on this study, it appears that the weakness of Modoki relative to canonical is dominant. More detailed observational analyses and modeling efforts are needed to verify this hypothesis.

The main conclusion of our study differs from that of *Rodrigues et al*. [2011], which is that SSTs in the equatorial and tropical South Atlantic tend to be lower during canonical events compared to Modoki. However,

© 2014. American Geophysical Union. All Rights Reserved.

Rodrigues et al. [2011] did show significantly more warming in the tropical North Atlantic in boreal winter and spring for canonical relative to Modoki, which is consistent with our results. The differences in the equatorial and tropical South Atlantic may stem from differences in the time period analyzed (1957–2002 in *Rodrigues et al*. [2011] compared to 1880–2010 in the present study) and the compositing technique (*Rodrigues et al*. [2011] based their composites on Northeast Brazil rainfall).

Previous studies have shown that canonical El Niños tend to suppress Atlantic hurricane activity in the boreal summer and fall [e.g., *Goldenberg and Shapiro*, 1996; *Klotzbach*, 2011a]. In addition, fluctuations in the tropical Atlantic north-south SST gradient (i.e., the Meridional Mode) have been linked to hurricane activity and to changes in rainfall over Africa and South America [*Kossin and Vimont*, 2007; *Hastenrath and Heller*, 1977]. Consistent with our results, *Larson et al*. [2012] showed that SSTAs in the tropical Pacific associated with noncanonical events are too weak to induce the increases in wind shear and atmospheric static stability in the tropical Atlantic that are necessary to suppress hurricane activity during the boreal summer and fall.

Recent studies indicate a growing frequency of Modoki ENSO events relative to canonical events in recent years [*Yeh et al*., 2009; *Ashok et al*., 2007; *Kao and Yu*, 2009; *Kug et al*., 2009; *Lee and McPhaden*, 2010]. Further, *Lee and McPhaden*, [2010] showed a growing intensity of central Pacific warming events during the past decade, though later studies indicate that this trend likely arises from unresolved natural decadal variability [*McPhaden et al*., 2011; *Yeh et al*., 2011]. Based on the results of this study, increases in the frequency and intensity of Modoki events, whether related to climate change or natural decadal variability, would tend to diminish the remote warming in the tropical Atlantic during boreal winter through summer. This may also lead to anomalous cooling in the northeastern tropical Atlantic during boreal spring and summer. *Klotzbach* [2011b] found a significant positive correlation between SST in the northeastern tropical Atlantic during June-July and tropical cyclone activity during the peak of the season (August-October). Anomalous cooling caused by Modoki events may therefore result in suppressed Atlantic hurricane activity relative to that experienced during canonical events. There remain uncertainties regarding the changing nature of El Niño and its impact on tropical Atlantic SSTs and hence tropical cyclone activity and South American and African rainfall. Understanding noncanonical El Niño phenomena and their teleconnections should therefore be a high priority for future research.

Acknowledgments

This research was conducted while DA participated in a summer internship at NOAA/AOML while holding a NOAA Ernest F. Hollings Scholarship at Texas A&M University. The authors thank the Physical Oceanography Division of AOML for partial funding of this work. Sang-Ki Lee made several valuable comments and suggestions during the course of the study. We thank Philip *Klotzbach*, Mike McPhaden, and an anonymous reviewer for comments that improved the quality of the paper.

References

Ashok, K., et al. (2007), El Niño Modoki and its possible teleconnection, *J. Geophys. Res.*, *112*, C11007, doi:10.1029/2006JC003798.

Barnston, A. G., and R. E. Livezey (1987), Classification, seasonality and persistence of low-frequency atmospheric circulation patterns, *Mon. Weather Rev.*, *115*, 1083–1126.

Bjerknes, J. (1969), Atmospheric teleconnections from the equatorial Pacific, *Mon. Weather Rev.*, *18*, 820–829.

Brown, R. G., and C. S. Bretherton (1997), A test of the strict quasi-equilibrium theory on long time and space scales, *J. Atmos. Sci.*, *54*, 624–638.

Carton, J. A., X. H. Cao, B. S. Giese, and A. M. daSilva (1996), Decadal and interannual SST variability in the tropical Atlantic Ocean, *J. Phys. Oceanogr.*, *26*, 1165–1175.

Chiang, J. C. H., and B. R. Lintner (2005), Mechanisms of remote tropical surface warming during El Niño, *J. Clim.*, *18*, 4130–4149.

Chiang, J. C. H., and A. H. Sobel (2002), Tropical tropospheric temperature variations caused by ENSO and their influence on the remote tropical climate, *J. Clim.*, *15*, 2616–2631.

Chiang, J. C. H., and D. J. Vimont (2004), Analogous Pacific and Atlantic meridional modes of tropical atmosphere–ocean variability, *J. Clim.*, *17*, 4143–4158, doi:10.1175/JCLI4953.1.

Chiang, J. C. H., Y. Kushnir, and A. Giannini (2002), Deconstructing Atlantic Intertropical Convergence Zone variability: Influence of the local cross-equatorial sea surface temperature gradient and remote forcing from the eastern equatorial Pacific, *J. Geophys. Res.*, *107*(D1), 4004, doi:10.1029/2000JD000307.

Compo, G. P., et al. (2011), The twentieth century reanalysis project, *Q. J. R. Meteorol. Soc.*, *137*, 1–28, doi:10.1002/qj.776.

Czaja, A., P. Van der Vaart, and J. Marshall (2002), A diagnostic study of the role of remote forcing in tropical Atlantic variability, *J. Clim.*, *15*, 3280–3290.

Enfield, D. B., and Mayer, D. A. (1997), Tropical Atlantic sea surface temperature variability and its relation to El Niño Southern Oscillation, *J. Geophys. Res.*, *102*(C1), 929–945, doi:10.1029/96JC03296.

Foltz, G. R., and M. J. McPhaden (2006), The role of oceanic heat advection in the evolution of tropical North and South Atlantic SST anomalies, *J. Clim.*, *19*, 6122–6138.

Gill, A. E. (1980), Some simple solutions for heat-induced tropical circulation, *Q. J. R. Meteorol. Soc.*, *106*, 447–462.

Goldenberg, S. B., and L. J. Shapiro (1996), Physical mechanisms for the association of El Niño and West African rainfall with Atlantic major hurricane activity, *J. Clim.*, *9*, 1169–1187.

Hastenrath, S., and L. Heller (1977), Dynamics of climatic hazards in northeast Brazil, *Q. J. R. Meteorol. Soc.*, *103*, 77–92, doi:10.1002/qj.49710343505.

Horel, J. D., and J. M. Wallace (1981), Planetary-scale atmospheric phenomena associated with the Southern Oscillation, *Mon. Weather Rev.*, *109*, 813–829.

© 2014. American Geophysical Union. All Rights Reserved.

Kao, H.-Y., and J.-Y. Yu (2009), Contrasting eastern-Pacific and central-Pacific types of ENSO, *J. Clim.*, *22*, 615–632, doi:10.1175/2008JCLI2309.1.
Kiladis, G. N., and H. F. Diaz (1989), Global climatic anomalies associated with extremes in the Southern Oscillation, *J. Clim.*, *2*, 1069–1090.
Klotzbach, P. J. (2011a), El Niño–Southern Oscillation's impact on Atlantic basin hurricanes and U.S. landfalls, *J. Clim.*, *24*, 1252–1263, doi:10.1175/2010JCLI3799.1.
Klotzbach, P. J. (2011b), A simplified Atlantic basin seasonal hurricane prediction scheme from 1 August, *Geophys. Res. Lett.*, *38*, L16710, doi:10.1029/2011GL048603.
Kossin, J. P. and D. J. Vimont (2007), A more general framework for understanding Atlantic hurricane variability and trends, *Bull. Amer. Meteorol. Soc.*, *88*, 1767–1781.
Kug, J.-S., F.-F. Jin, and S.-I. An (2009), Two types of El Niño events: Cold tongue El Niño and warm pool El Niño, *J. Clim.*, *22*, 1499–1515, doi:10.1175/2008JCLI2624.1.
Larson, S., et al. (2012), Impacts of non-canonical El Niño patterns on Atlantic hurricane activity, *Geophys. Res. Lett.*, *39*, L14706, doi:10.1029/2012GL052595.
Lee, S.-K., D. B. Enfield, and C. Wang (2011), Future impact of differential inter-basin ocean warming on Atlantic hurricanes, *J. Clim.*, *24*, 1264–1275, doi:10.1175/2010JCLI3883.1.
Lee, T., and M. J. McPhaden (2010), Increasing intensity of El Niño in the central-equatorial Pacific, *Geophys. Res. Lett.*, *37*, L14603, doi:10.1029/2010GL044007.
McPhaden, M. J., T. Lee, and D. McClurg (2011), El Niño and its relationship to changing background conditions in the tropical Pacific Ocean, *Geophys. Res. Lett.*, *38*, L15709, doi:10.1029/2011GL048275.
Messié, M., and F. Chavez (2011), Global modes of sea surface semperature variability in relation to regional climate indices, *J. Clim.*, *24*, 4314–4331, doi:10.1175/2011JCLI3941.1.
Rodrigues, R. R., R. J. Haarsma, E. J. D. Campos, and T. Ambrizzi (2011), The impacts of inter-El Niño variability on the tropical Atlantic and Northeast Brazil climate, *J. Clim.*, *24*, 3402–3422.
Smirnov, D., and D. J. Vimont (2012), Extratroical forcing of tropical Atlantic variability during boreal summer and fall, *J. Clim.*, *25*, 2056–2076.
Smith, T. M., and R. W. Reynolds (2003), Extended reconstruction of global sea surface temperatures based on COADS Data (1854–1997). *J. Clim.*, *16*, 1495–1510, doi:10.1175/1520-0442-16.10.1495.
Smith, T. M., et al. (2008), Improvements to NOAA's historical merged land-ocean surface temperature analysis (1880–2006), *J. Clim.*, *21*, 2283–2296, doi:10.1175/2007JCLI2100.1.
Tang, B. H., and J. D. Neelin (2004), ENSO Influence on Atlantic hurricanes via tropospheric warming, *Geophys. Res. Lett.*, *31*, L24204, doi:10.1029/2004GL021072.
Tanimoto, Y., and S. P. Xie (2002), Inter-hemispheric decadal variations in SST, surface wind, heat flux, and cloud cover over the Atlantic Ocean, *J. Meteorol. Soc. Jpn.*, *80*, 1199–1219.
Tedeschi, R. G., I. F. A. Cavalcanti, and A. M. Grimm (2013), Influences of two types of ENSO on South American precipitation, *Int. J. Climatol.*, *33*, 1382–1400, doi:10.1002/joc.3519.
Trenberth, K. E., and D. P. Stepaniak (2001), Indices of El Niño evolution, *J. Clim.*, *14*, 1697–1701.
Tziperman, E., et al. (1998), Locking of El Niño's peak time to the end of the calendar year in the delayed oscillator picture of ENSO, *J. Clim.*, *11*, 2191–2199.
Vimont, D. J. (2010), Transient growth of thermodynamically coupled variations in the tropics under an equatorially symmetric mean, *J. Clim.*, *23*, 5771–5789.
Wallace, J. M., and D. S. Gutzler (1981), Teleconnections in the geopotential height field during the Northern Hemisphere Winter, *Mon. Weather Rev.*, *109*, 784–812.
Yeh, S.-W., B. P. Kirtman, J.-S. Kug, W. Park, and M. Latif (2011), Natural variability of the central Pacific El Niño event on multi-centennial timescales, *Geophys. Res. Lett.*, *38*, L02704, doi:10.1029/2010GL045886.
Yeh, S.-W., J.-S. Kug, B. Dewitte, M.-H. Kwon, B. P. Kirtman, and F.-F. Jin (2009), El Niño in a changing climate, *Nature*, *461*, 511–514, doi:10.1038/nature08316.
Yulaeva, E., and J. M. Wallace (1994), The signature of ENSO in global temperature and precipitation fields derived from the microwave sounding unit, *J. Clim.*, *7*, 1719–1736.

© 2014. American Geophysical Union. All Rights Reserved.